Asymmetry Analysis in Rodent Cerebral Ischemia Models[1]

Sheena Xin Liu, MS, MD, PhD, Celina Imielinska, PhD, Andrew Laine, PhD, William S. Millar, MD, MS
E. Sander Connolly, MD, Anthony L. D'Ambrosio, MD

Rationale and Objectives. An automated method for identification and segmentation of acute/subacute ischemic stroke, using the inherent bi-fold symmetry in brain images, is presented. An accurate and automated method for localization of acute ischemic stroke could provide physicians with a mechanism for early detection and potentially faster delivery of effective stroke therapy.

Materials and Methods. Segmentation of ischemic stroke was performed on magnetic resonance (MR) images of subacute rodent cerebral ischemia. Eight adult male Wistar rats weighing 225–300 g were anesthetized with halothane in a mix of 70% nitrous oxide/30% oxygen. Animal core temperature was maintained at 37°C during the entire surgical procedure, including occlusion of the middle cerebral artery (MCA) and the 90-minute post-reperfusion period. To confirm cerebral ischemia, transcranial measurements of cerebral blood flow were performed with laser-Doppler flowmetry, using 15-mm flexible fiberoptic Doppler probes attached to the skull over the MCA territory. Animal MR scans were performed at 1.5 T using a knee coil. Three experts performed manual tracing of the stroke regions for each rat, using the histologic-stained slices to guide delineation of stroke regions. A strict tracing protocol was followed that included multiple (three) tracings of each stroke region. The volumetric MR image data were processed for each rat by computing the axis of symmetry and extracting statistical dissimilarities. A nonparametric Wilcoxon rank sum test operating on paired windows in opposing hemispheres identified seeds in the pixels exhibiting statistically significant bi-fold mirror asymmetry. Two brain reference maps were used for analysis: an absolute difference map (ADM) and a statistical difference map (SDM). Although an ADM simply displays the absolute difference by subtracting one brain hemisphere from its reflection, SDM highlights regions by labeling pixels exhibiting statistically significant asymmetry.

Results. To assess the accuracy of the proposed segmentation method, the surrogate ground truth (the stroke tracing data) was compared to the results of our proposed automated segmentation algorithm. Three accuracy segmentation metrics were utilized: true-positive volume fraction (TPVF), false-positive volume fraction (FPVF), and false-negative volume fraction (FNVF). The mean value of the TPVF for our segmentation method was 0.8877; 95% CI 0.7254 to 1.0500; the mean FPVF was 0.3370, 95% CI −0.0893 to 0.7633; the mean FNVF was 0.1122, 95% CI −0.0502 to 0.2747.

Conclusions. Unlike most segmentation methods that require some degree of manual intervention, our segmentation algorithm is fully automated and highly accurate in identifying regions of brain asymmetry. This approach is attractive for numerous neurologic applications where the operator's intervention should be minimal or null.

Key Words. Abnormality segmentation; brain symmetry; nonparametric test; stroke detection; ischemia stroke.

© AUR, 2008

Stroke is the third leading cause of death in the United States, resulting in approximately 150,000 deaths per year (1). Building a computer-aided diagnostic tool that detects the presence or absence of an acute/subacute ischemic infarct could improve patient outcomes through earlier detection. An accurate, automated, and efficient method that identifies acute/subacute brain ischemia with magnetic resonance (MR) imaging could provide physicians with an additional tool for delivering fast and effective stroke therapy.

Automated detection and segmentation of brain abnormalities spans several decades of research (2). To facilitate fully automated segmentation, it is known that image information alone is insufficient to successfully differentiate among target organs, abnormal tissue, and the background (3). For example, the active contour classification (4) and simple fuzzy connectedness (5) methods require manual selection of seeds to initialize the segmentation process. Some existing fully automated methods experience other shortcomings. For example, statistical classification methods (6) may fail when a brain lesion shows insufficient contrast against its background or presents highly inhomogeneous patterns. Inhomogeneity results in overlapping intensity distributions between healthy tissue and abnormal tissue.

In atlas-based segmentation methods, structure features and relationships between the structures in the normal brain anatomy are used to guide the classification of different tissue types (7). Kaus et al (3) proposed an adaptive method that combines statistical classification with anatomic knowledge. The algorithm involves an iterative process of classification and nonlinear registration to match the anatomic templates from a digital atlas with the brain anatomy of the patient. In most knowledge-driven classification methods, however, bilateral symmetry, which might provide additional information about brain pathology, has not been used. To combine knowledge-driven classification with properly represented and encoded symmetry information is very challenging.

Thirion et al (8) proposed a method that estimates three-dimensional (3D) dissymmetry fields that makes use of 3D vector field operators and computes significance maps in processing brain pathologies. There are three main application fields: the study of the normal dissymmetry within a given population, the comparison of the dissymmetry between two populations, and the detection of the significant abnormal dissymmetry of a patient with respect to a reference population. However, the results are presented for qualitative rather than quantitative evaluation.

Volkau (9) evaluated asymmetry as a global scalar measure, using Jeffrey's divergence measure (J-divergence) to classify brain pathologies. This approach is limited because the algorithm uses a single threshold value as the classifier, which may lead to false classification of asymmetries in other normal tissue structures, such as the skull, eye, nose, and cerebral vasculature as pathologies.

In this work, we propose a method to identify and segment brain pathologies using the inherent bi-fold symmetry in brain imagery. The main feature of this novel approach is the replacement of the spatial prior, which is a generic statistically normal human brain atlas, with the patient-specific left-to-right symmetry information derived from the patient's own brain images. This framework accurately captures asymmetries between hemispheres and quantifies discrepancies between them. To demonstrate capabilities of our approach, in a chosen clinical application, we propose a fully automated and accurate method of detecting subacute ischemic stroke.

Radiologists use symmetry as one of the discriminating features to help detect and analyze brain pathology. Based on the assumption that the brain exhibits a high level of bilateral symmetry and that this symmetry is violated by pathologic conditions, we use the healthy side of the brain as a template to capture statistically significant hemisphere-wise differences. Our algorithm, in essence, repeats quantitatively, the radiologist's examination and comparison of the opposing hemispheres.

MATERIALS AND METHODS

All procedures performed on animals were approved by the Columbia University Institutional Animal Care and Use Committee and were carried out according to institutional and federal guidelines. Eight adult male Wistar rats, ranging in weight from 225–300 g, were anesthetized with halothane in a mix of 70% nitrous oxide/30% oxygen. Animal core temperature was maintained at 37°C during the entire surgical procedure, including occlusion of the middle cerebral artery (MCA) and the 90-minute post-reperfusion period (10). A mid-line neck incision was created to expose the right carotid sheath during the operation. Ischemic stroke in the territory of the MCA was accomplished by advancing a 25 mm 4-0 nylon suture with a 0.38-mm outer diameter cast rubber tip until the tip occluded the MCA. The occluding suture was removed after 120 minutes of ischemia. To confirm cerebral
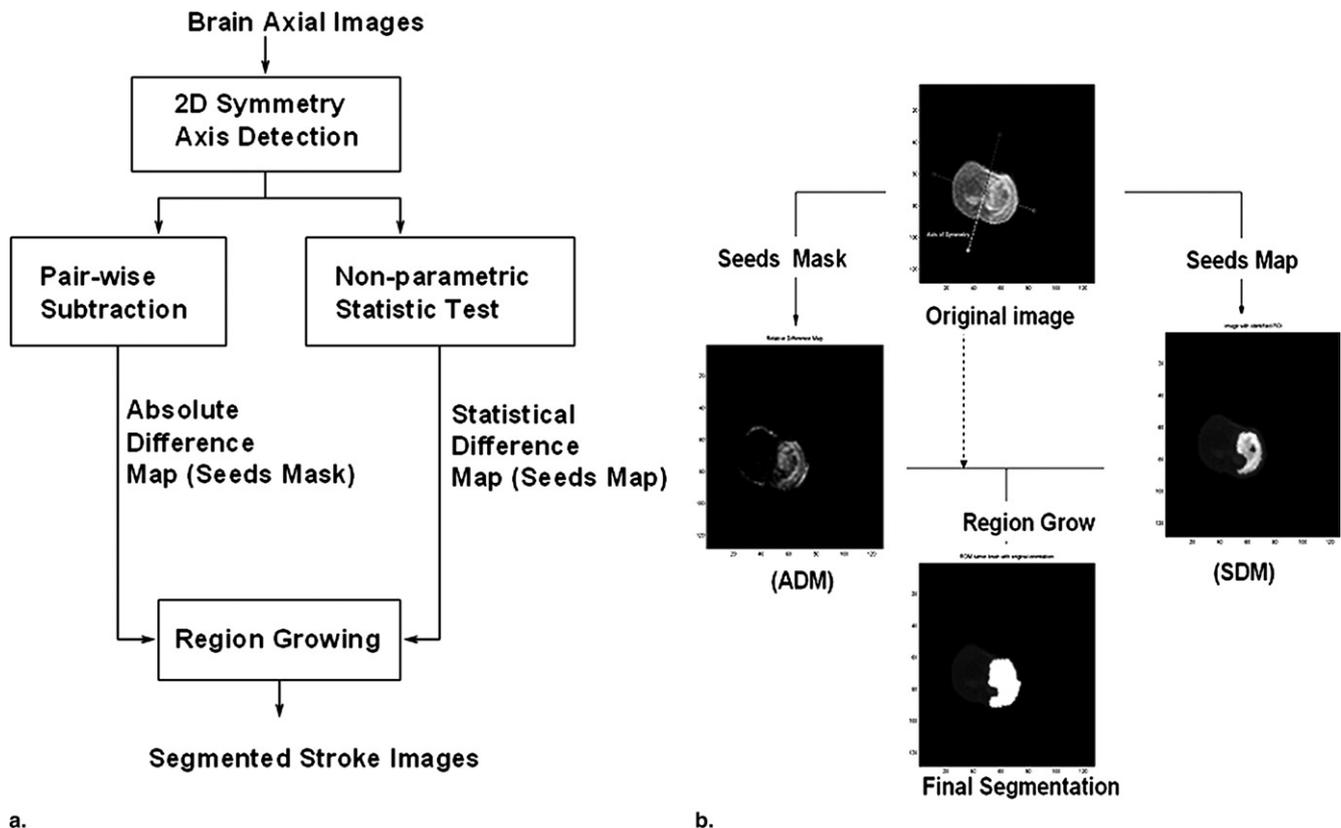
Figure 1. The proposed segmentation framework is demonstrated in a flowchart **(a)** and a graphic illustration **(b)** in segmenting stroke from rat ischemia stroke models in magnetic resonance imaging. 2D, two dimensional; ADM, absolute difference map; SDM, statistical difference map.

ischemia, transcranial measurements of cerebral blood flow were made with laser-Doppler flowmetry using 15-mm flexible fiberoptic Doppler probes attached to the skull over the MCA territory. Reduction of laser-Doppler flowmetry readings to at least 40% of baseline was defined as adequate cerebral blood flow dropoff. On day 7 postischemia, all eight rats were anesthetized and MR imaged at 1.5 T with a knee coil. Immediately after MR imaging, the rats were sacrificed; the brains were removed intact and placed in a brain matrix (Harvard Apparatus) (11) for postmortem histologic analysis with 2-mm coronal sectioning. We validated our method using ground truth data that were collected from this rat model, under our earlier project, as previously reported (12). All MR images were stored in Digital Imaging and Communications in Medicine (DICOM) format for postprocessing and segmentation analysis. We run our algorithm using MATLAB computing environment in a 512M RAM, Windows XP platform (Microsoft, Redmond, Washington), with Intel T2500 2.0 GHz Core Duo processor (Intel, Santa Clara, California).

Approach Overview

We propose a symmetry-based approach to detect and segment brain pathologies consisting of the following modules: computation of axis of symmetry of brain structure, statistical extraction of the seeds for growing, and region growing and segmentation of the target pathology (Fig 1). We make an assumption that the brain is often nearly symmetric and that this symmetry is violated under pathologic conditions. By detecting the symmetry axis and secondarily quantifying any hemispheric asymmetries, we may identify and quantify pathologic conditions.

Before we can identify and quantify these asymmetries, we must first solve two technical problems. First, not all head MR images are perfectly aligned within the scanner coordinate system. Therefore, we have to follow the actual orientation of the subject's head/brain and identify the axis of symmetry in each individual slice in the acquired volumetric data. Second, the detection of subtle-to-gross pathologic asymmetries in the brain may be disturbed by normal variations between the left and right brain hemispheres, the degree of which can also vary be-
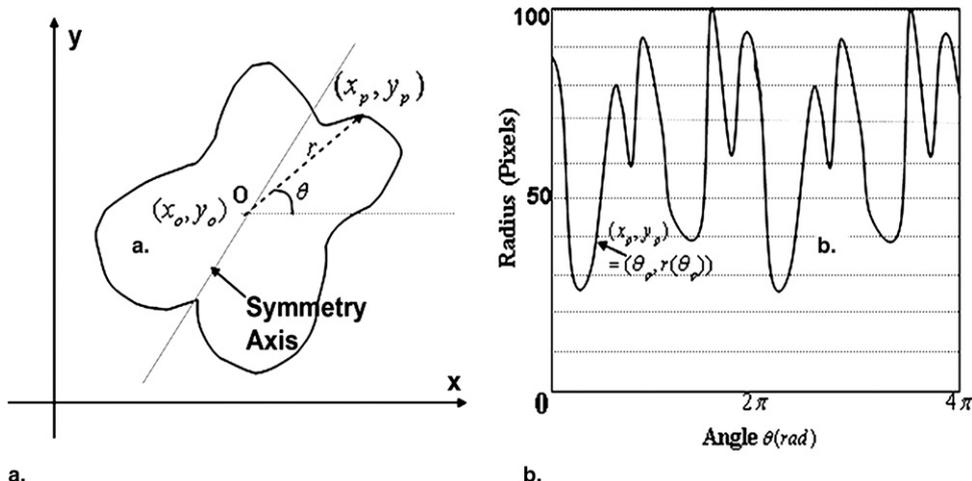
Figure 2. **(a)** The axis of symmetry in an almost symmetric object. Each point has been reparameterized by its radius R and the angle θ. **(b)** In r-θ polar space, we seek the global minimum of the symmetry measure—the sum of element-by-element absolute difference—between two adjacent windows of size π.

tween patients. We claim that, in the majority of brain images, normal asymmetries are less dramatic than the abnormal ones. Working under this assumption, the evaluation of apparent bilateral asymmetries in brain images using a nonparametric statistical test and operating on paired small windows, potentially can distinguish between normal and gross pathologic asymmetries. We define two types of maps that will facilitate the statistical evaluation: the statistical difference map (SDM) and the absolute difference map (ADM). The SDM highlights regions in a statistical sense, labeling pixels with statistically sufficient asymmetry as good candidates for the seeds of the pathologies. The ADM simply displays the absolute difference by subtracting one hemisphere from its reflection. The seeds identified in the SDM are iteratively aggregated within the ADM, yielding the segmentation of an abnormal target in the brain. These two maps are cross-referenced through adaptive region growing; the SDM provides the seeds and the ADM plays the role of a mask for pixels that the algorithm uses for region growing. This is depicted in the flowchart in Figure 1. The final output of the process is the segmented object that precisely delineates and quantifies the pathologic regions presenting with poor symmetries. The quality of asymmetry quantification is based on the correct derivation of the ADM and the SDM, which, in turn, strongly depends on the correct identification of the symmetry axis. These two critical steps in the segmentation process are addressed in the following sections.

Detection of the Symmetry Axis for each Individual Scan

Various approaches for detecting, analyzing, and measuring two-dimensional symmetry in image processing have been suggested (13–15). In our early work (16), the following algorithm for detecting the symmetry axis of a two-dimensional planar shape was presented.

Let us assume that we have a single region of interest (the brain), R. Given the region of interest R within the image I, where δ is the background cutoff that separates background from the head, we assign a very small value to δ, because the background intensity in most image modalities is close to zero. X_R, the characteristic function $X_R: I \rightarrow (0,1)$ can be calculated as follows:

$$X_R(x, y) = \begin{cases} 1 & if\ (x, y) \in R : I(x, y) > \delta \\ 0 & \text{otherwise} \end{cases}.$$

With the integration over the whole image I, the area is defined as the 0th moment of R. Then the centroid $C = (\bar{x}, \bar{y})$ is computed, as detailed elsewhere (17).

For an object with a well-defined boundary, there are lines extending from the centroid $(\bar{x}, \bar{y})$ with direction θ and length $r(\theta)$. We map this object to r-θ polar space, which gives rise to a new image $I(r, \theta)$, where the origin (0,0) in polar coordinates (Fig 2b) corresponds to the centroid in the Cartesian coordinates (Fig 2a). Any axis passing through the centroid of this object can be uniquely specified in polar space expressed as $\theta = \varphi$. In polar rep-

resentation, to determine a mirror symmetry axis, we seek the φ value that minimizes the sum of the absolute distance between two adjacent windows of size π:

$$d_\phi(R_0, L_0) = \int_{\theta=0}^{\pi} \left| r(\varphi + \theta) - r(\varphi - \theta) \right| d\theta$$

with the symmetry axis being $\varphi_\tau = \arg \min d_\phi(R_0, L_0)$.

The resulting φ_τ represents the global minimum of the distance function $d\varphi$ in the polar space. φ_τ uniquely specifies the symmetry axis, and the parametric form of this line in the Cartesian coordinates is $x = \bar{x} + t \cos(\varphi_\tau)$, $y = \bar{y} + t \sin(\varphi_\tau)$ (Fig 2a).

Generation of the SDM and ADM

After detecting the axis of symmetry, the brain image can be checked for significant differences in regions geometrically co-located relative to the axis of symmetry. This defines the essence of the symmetry-based paradigm documented in our previous publications (18,19), but used in different applications. In this work, instead of employing the relative difference map (18), which was used for computing relative differences in intensities in two symmetric small windows in corresponding brain hemispheres, expressed in normalized difference (a ratio between 0 and 1), we refine the method and capture pathologic asymmetry by looking at the statistical significance level (P value) of the detected difference.

The statistical test provides the "likelihood" of the difference to appear, by chance, between given paired samples. This means that the difference has 1: N chance of occurrence *without* underlying asymmetry being present. SDM extracts regions with significant hemisphere-wise difference that generates preliminary seeds, and those seeds are later aggregated under certain similarity criteria, using an adaptive region growing algorithm, until it includes all the pixels of damaged tissue. This completes the final segmentation of the target pathologic region. Unlike many existing region growing methods, the seed placement in out algorithm is fully automated.

The Statistical Difference Map

The symmetry axis separates the brain into two hemispheres. We denote a reoriented and recentered two-dimensional image as $X(r_x, c_y)$, where $r_x \in \{1, 2, .. N_Y\}$, $c_y \in \{1, 2, .. N_X\}$, and N_X, N_Y are the x, y dimensions of each scan. In the realigned brain along the symmetry axis $c_{sym} = N_X/2$, the image is split into two halves according to the symmetry axis. We denote the left and right hemispheres as X_L and X_R, respectively.
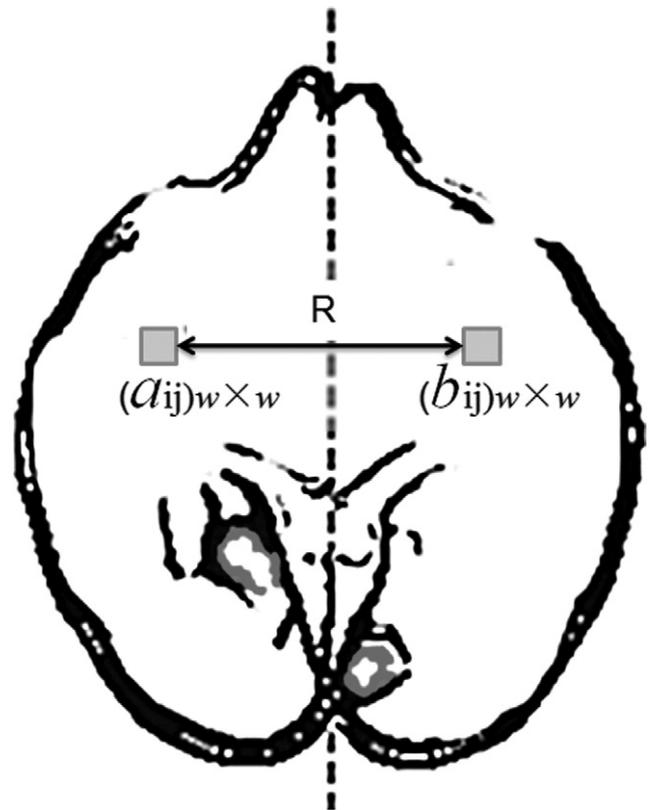
Figure 3. Statistical significance test is performed based on two paired windows as the sample units.

The neighborhood of a pixel is defined as the set of offsets both in columns and rows from this pixel, as shown below in Equation 1. It defines a vicinity of the point (r_x, c_y) of image X:

$$S_N : X(r_x, c_y) = \{X(r_x, c_y) : (r_x + \Delta r, c_y + \Delta c), \\ \times (\Delta r, \Delta c) \in N\}. \quad (1)$$

We set the square-shaped neighborhood, with window size $w = \Delta r = \Delta c$ as one sample unit (Fig 3). Therefore, two windows, $(a_{i,j})_{w \times w}$, $(b_{i,j})_{w \times w}$, from the hemispheres X_L and X_R form two sample units, $1 \le i \le w$, $1 \le j \le w$. We slide each of the two windows across the entire half of the image and conduct statistical analysis sequentially, window by window. We set the window size $w = 7$ and apply Wilcoxon's rank sum test (20), denoted as k, on the paired sample units for a given significance level α. This returns a P value as shown in Equation 2.

$$\left[h(r_x, c_y), p(r_x, c_y)\right] = k\left(\{S_N : X_L(r_x, c_y), S_N : X_R(r_x, c_y), \alpha\}\right). \quad (2)$$

We use a nonparametric statistic analysis to test if two populations have the same continuous distribution, for two reasons: the sample size is not sufficiently big for performing a parametric statistical test (explained later), and we cannot assume that the population within each square window is normally distributed. The Wilcoxon rank sum test is a standard nonparametric test that is based on ranks. All the sample data are merged and each pixel value is ranked from the lowest to the highest. All sequences of ties are assigned an average rank. The null hypothesis $h(r_x, c_y)$ is that no statistical difference exists between paired windows on two hemispheres. The null hypothesis is rejected if, in the ranking, all the pixels in one window rank sufficiently higher than all the pixels in the other window. The level of significance, α, indicates the probability that one window ranks significantly higher than the other, whereas under the null hypothesis no difference exists between the two populations, where α is a P value between 0 and 1. The smaller the returned P value is, the less likely that the two populations have the same continuous distribution. If the returned P value is less than the preset significant value α, then the null hypothesis is rejected. By decreasing α to a small value, we reject the null hypothesis so that the majority of the paired windows are considered of no significant statistical difference. Otherwise, the SDM would overselect regions containing normal tissue—asymmetric clusters of pixels. Our aim is to detect the minimal necessary asymmetries and identify them as seeds. We define h as a binary decision mask that assigns to all pixels a value of 1 if they exhibit a significant difference, given the predefined level of significance α. SDM performs a statistical test that returns h as a binary value, with h equal to 1 corresponding to the null hypothesis being rejected. We herein obtain a new characteristic function $X_\alpha(r_x, c_y)$ based on the value of α, $X_\alpha: X(r_x, c_y) \rightarrow \{0, 1\}$. This function is shown in Equation 3:

$$X_\alpha(r_x, c_y) = \begin{cases} 1, \forall (r_x, c_y) : h(r_x, c_y) = 1 \; given \; \alpha \\ 0, \; otherwise \end{cases}. \quad (3)$$

If there is a significant normal variation between hemispheres, it is highly likely that the method will capture both pathologic abnormalities and artifacts coming from normal asymmetries. The presence of normal and pathologic asymmetries makes it essential to introduce an additional threshold that will allow for differentiation between these two types of asymmetries.

In the brain image, we exclude areas where $X_\alpha(r_x, c_y) = 1$ (candidate stroke area), and use the average of the intensities of the rest of the brain, ± 1.96 standard deviation (SD) (nonstroke area) as a cutoff to remove the possible artifacts. The falsely captured, normal tissue, asymmetric regions, under our assumptions, through statistical difference computation, can be enclosed within the value range of the normal brain tissues, and excluded. The resulting image is binary, defined in Equation 4:

$$X_\alpha(r_x, c_y) = 0, \; if \; X_\alpha(r_x, c_y) = 1 \cap X(r_x, c_y) < \varepsilon \quad (4)$$

$X_\alpha(r_x, c_y)$ is a refined binary image where 1s show the pathologic asymmetric regions and 0s indicate normal brain tissue. Theoretically, $X_\alpha(r, c)$ should be perfectly symmetric with respect to the symmetry axis, because one P value is produced from one paired windows test. However, we only identify the area in the brain hemisphere on the side of the stroke occurrence. This yields the SDM, also named as the seeds map (Fig 1, Fig 4c). In rat ischemia MR images, pixels in the stroke region exhibit hyperintensity relative to that of the normal brain tissue. The *seeds* generated by the SDM would only appear on the pathologic side of the brain. Therefore, we define the SDM *(seeds map)*, in Equation 5, corresponding to the side of the brain with the stroke that is identified and highlighted. This map produces an initial underestimation of a stroke region. Because it is binary, 1s and 0s represent pixels in regions that statistically correspond to high and low likelihood of stroke, respectively. The reason *SDM* generates undersegmented stroke regions is that, while eliminating the possible artifacts introduced by normal bilateral asymmetries and unilateral or inhomogeneous data acquisition noise, we may also eliminate marginal areas of the stroke region.

$$SDM(r_x, c_y) = \begin{cases} X_\alpha(r_x, c_y), & I_{S_N:X(r,c)} > I_{S_N:X_{opp}(r,c)} \\ 0 & otherwise \end{cases}. \quad (5)$$

The ADM

The $ADM(r_x, c_y)$ is defined as:

$$ADM(r_x, c_y) = \left[\|X_L - X_R\|, f(\|X_L - X_R\|)\right]. \quad (6)$$

ADM computes the absolute difference between two hemispheres, where f denotes the left–right flip function
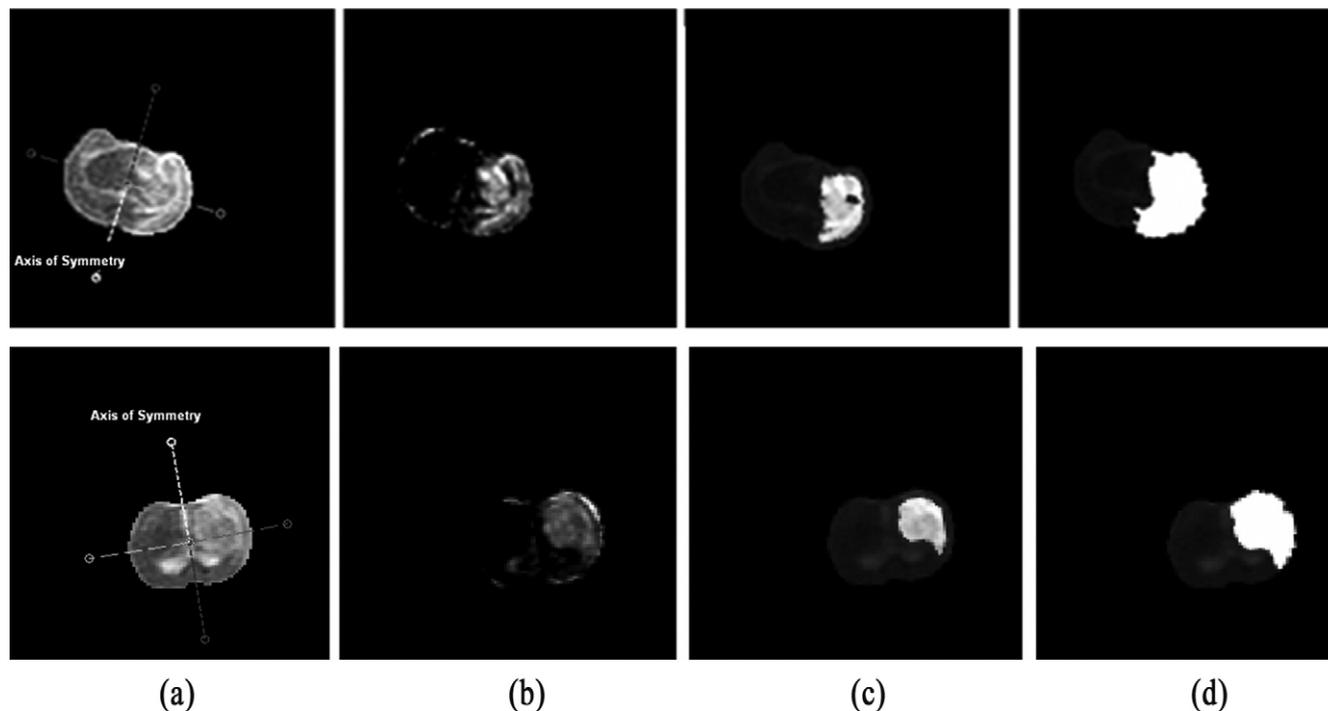
Figure 4. Ischemic stroke segmentation from magnetic resonance imaging rat images. **(a)** The original images; **(b)** the absolute difference map; **(c)** the statistical difference map (a small empirical *P* value is chosen); and **(d)** final segmented images after region growing operation.

along the x axis. From definition (Eq. 6), ADM is expected to be symmetric with respect to the axis of symmetry. ADM provides the reference image from where the seeds propagate. We also refer it as the seeds mask (Fig 1, Fig 4b).

Region growing within the difference map.—The basic idea behind *region growing* is to aggregate pixels (voxels) that are adjacent and belong to the same tissue type with fairly homogeneous grayscale properties (21). The region growing approach consists of two main steps: 1) selecting a set of seed points and 2) growing the region by appending the neighboring pixels (voxels) that have satisfied similarity criteria. In our segmentation pipeline, the seeds have been drawn from the preceding steps. The "seeds" can be defined as the clusters of pixels with the most statistically significant asymmetries, and their selection, as explained earlier, is fully automated. The stopping criteria for region growing are formulated dynamically based on the mean and SD of a currently grown region. It is assumed that the population of the seeds is normally distributed with a mean and standard error (SE). $SE = SD/\text{sqrt}(n - 1)$. SD is the SD of n number of seed points. The mean, ± 1.96 times the SE, provides the 95% confidence level. This corresponds to a finding of significance at the 0.05 level when the hypothesized mean is outside the 95% confidence limits around the sample mean.

This corresponds to a 0.05 chance that a sampled case will lie greater than 1.96 SDs from the mean where the value of each candidate pixel is compared to the average intensity of the seed region grown. If it falls into the inclusion of 95% confidence interval (CI), the candidate is counted as a new seed.

Thus, the threshold value is used to test if the candidate is sufficiently similar to the seeds. This step is iterated until convergence. In summary, the region from the seeds map is being grown within the seed mask and a threshold value has been automatically determined based on the statistical properties of the seeds already grown.

The output generated using our method is a labeled region, where the label indicates the membership of a pixel (voxel) in a segmented object (Fig 4a). A label of zero indicates that the voxel was not assigned to any object. In cases where the brain has multiple lesions, the segmented image has multiple distinctive non-zero labels.

RESULTS

We applied the proposed framework to segmenting ischemic stroke regions in the rat model. In identification
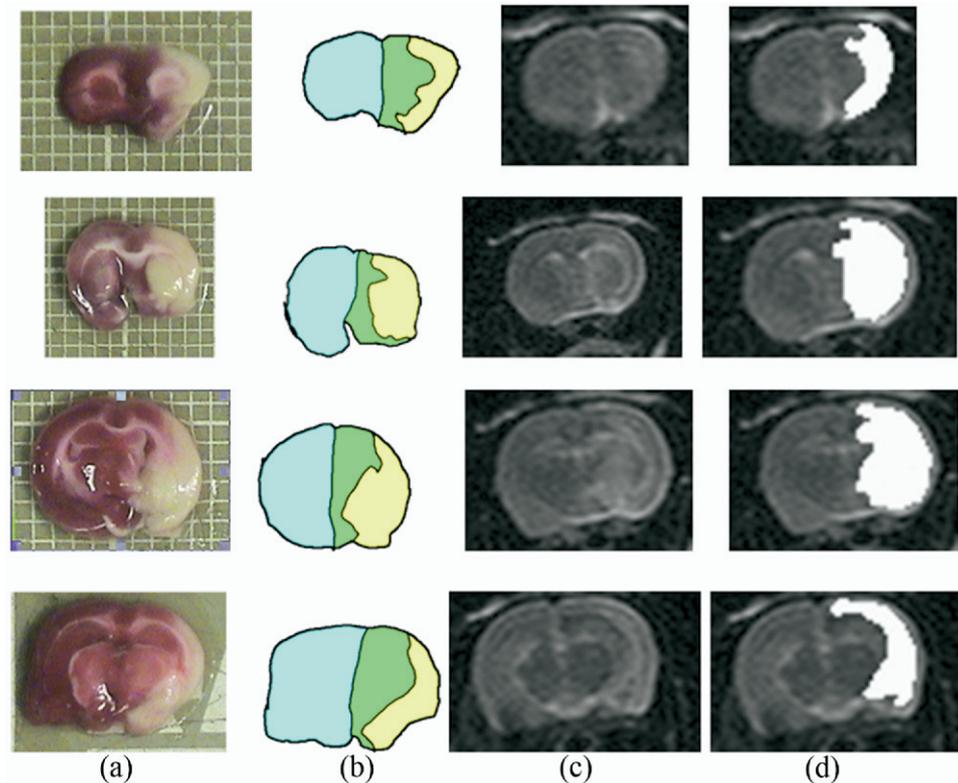
Figure 5. Delineation of stroke area in rat magnetic resonance (MR) data using histologic slices for guidance: **(a)** histologic data, **(b)** delineated stroke regions in histologic data, **(c)** MR data, and **(d)** delineated stroke regions in MR data (21).

and segmentation of brain stroke from the rat ischemia model, first the symmetry axis was found (Fig 4a). Figure 1 demonstrates the workflow of the symmetry-based approach. It consists of two parallel operations: generation of an SDM (seeds map) and generation of an ADM (seeds mask). The statistical difference map provides the initial seeds map (SDM) that is characterized as an undersegmented region of interest. The final segmented stroke area is obtained by growing the seeds within the seeds mask (ADM). We then evaluate the performance of the framework, comparing the segmentation result with that of the ground truth previously obtained from experts' hand delineations.

Development of Expert-based Ground Truth

We describe the process of generating ground truth, published in previous work. Three experts performed manual tracing of the stroke regions on MR imaging for each rat (22), following a strict protocol, and repeated it three times, using the histologic-stained slices to guide delineation of the stroke region (Fig 5). The multiple de-

lineations by the experts represent intra- and interexpert variability. The collection of MR rat ischemic stroke data has been hand segmented by three individual experts, leading to a partition of each image into two subregions: "abnormal" (stroke) and "normal" (nonstroke area). To evaluate the results, we asked three operators (two senior medical students and one trained technician) to segment the rat ischemia stroke manually three times on different occasions. For the purpose of this study, we selected four rats' MR imaging scans, and, for each rat, nine manual delineations of the ischemic stroke region were generated. Each rat had eight slices per volume. The nine delineations of abnormal ischemic stroke regions were combined to generate a "fuzzy" set of the surrogate of ground truth for the ischemic stroke region. In a fuzzy set, the membership to the set is assigned as a probability, whereas in a binary set the membership function is either true or false. We define probability as a floating number between 0 and 1, computed as ratio of the number votes from the hand delineations (by all the experts) labeled a pixel/ voxel as a lesion to the total number votes that corre-
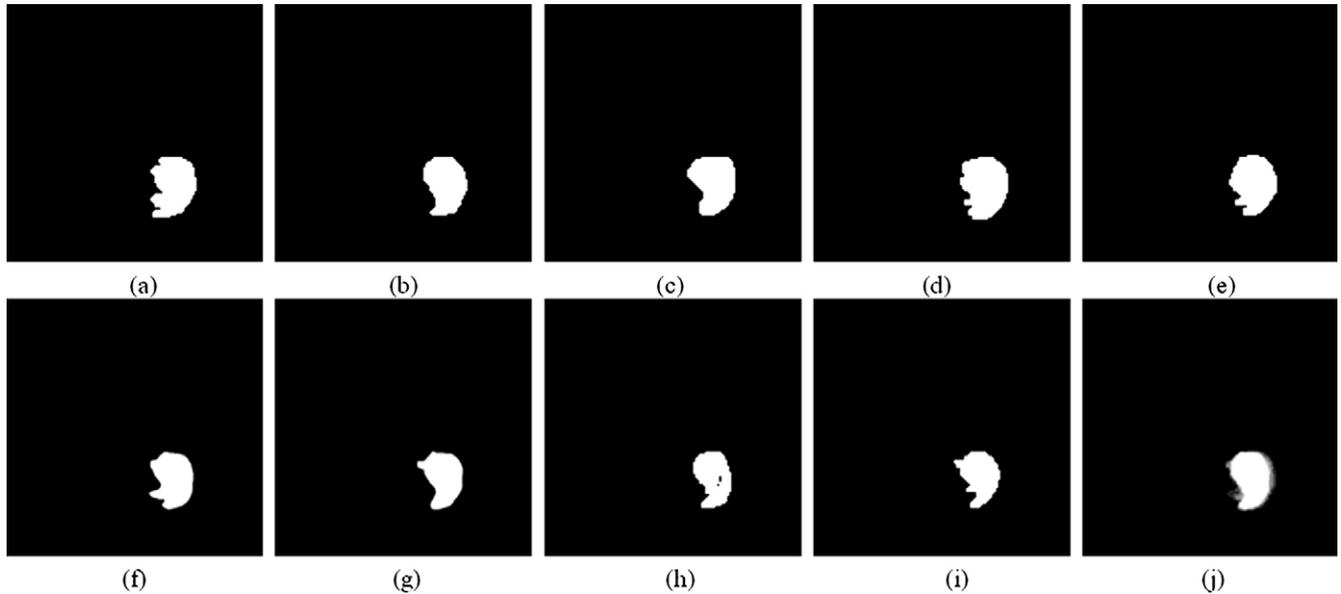
Figure 6. Surrogate ground truth derived from hand delineations of a single slice **(a–i)** nine S1–S9 hand-segmentations generated by experts. **(j)** The fuzzy object representing surrogate ground truth.

sponds to all hand delineations generated by the experts. For instance, the value 1 represents a region that all three operators, in all nine hand delineations, agree that a pixel/voxel belongs to a stroke region, whereas 0 means none of the operators consider it as a lesion pixel/voxel; then the value of a pixel/voxel may increase by 1/9 from 0 to 1. We show in Figure 6j a single slice surrogate ground that is obtained from nine segmentations (Fig 6a–i). Variability of experts' performance is measured by the coefficient of variation (CV). The CV represents the ratio of the SD to the mean; it is therefore a useful statistic to compare the degree of variation. Given that i is the ith number of trials of total n trials, each trial delineates an area of S_i, then the standard deviation (SD) of n times of trails is

$$SD = \sqrt{\frac{1}{n-1}\sum_{i=1}^{n}\left(S_i - S_0\right)}$$

therefore, the CV, $CV = SD/S_0$, where S_0 is the mean area of n trials and CV is coefficient of variation.

As demonstrated in Table 1, operator 3 performed most consistently, with a 3.21% intraoperator CV. The interoperator CV is high (19.08%). This is due to the difficulty in establishing the true delineation of the object of interest, even with the help of histologic stain. Table 2 summarizes the intra- and interoperator variabilities for those scans.

We have developed a comprehensive segmentation evaluation methodology (23) in a joint effort between University of Pennsylvania and Columbia University. We focus in this work on some aspects of the framework: the assessment of *accuracy* of our segmentation method, where accuracy represents agreement with the ground truth, and the assessment of efficiency.

Assessment of Accuracy

In Figure 7, we show sample results from the MR imaging ischemic stroke study that include four of eight rats. We performed quantitative analysis of accuracy of our method, using three metrics: truth-positive volume fraction (TPVF), false-positive volume fraction (FPVF), and false-negative volume fraction (FNVF) (23). Given S_T and S, which are sets of pixels representing segmentations from the ground truth and our algorithm, these accuracy measures are defined as follows.

$$TPVF(S, S_T) = \left|S_T \cap S\right|/\left|S_T\right|,$$
$$FPVF(S, S_T) = \left|S - S_T\right|/\left|S_T\right|,$$
$$FNVF(S, S_T) = \left|S_T - S\right|/\left|S_T\right|.$$

TPVF describes the fraction of the total amount of tissue with which the segmented stroke overlaps. *FPVF* denotes the fraction of the tissue falsely identified as the stroke. *FNVF* indicates the fraction of the tissue that was

Table 1
The Intra- and Interoperator Variabilities Between the Hand-segmented Delineations of the Stroke Region Affects the Reliability of the Resulting Surrogate Ground Truth

	Intra- and Interoperator Variabilities for One Rat Scan								
	Operator 1			Operator 2			Operator 3		
Segmentation	Trial 1	Trial 2	Trial 3	Trial 1	Trial 2	Trial 3	Trial 1	Trial 2	Trial 3
Ground truth area (pixel)	476.3								
Segmented area (pixel)	534	475	514	577	666	459	419	390	396
Area of difference	12.1%	0.29%	7.91%	21.13%	39.8%	6.39%	12.0%	18.1%	16.8%
TPVF	0.935	0.899	0.933	0.954	1	0.872	0.838	0.798	0.779
Intra CV		6.30%			21.80%			3.21%	
Inter CV					19.08%				

CV: coefficient of variation; TPVF: true-positive volume fraction.

The accuracy assessment of the automated segmentations is affected. The "experts" used in this project were trained medical students who have showed noticeable intra- and interoperator discrepancies quantified by CV. For a given rat scan, operator 1 has shown 6.30% intraoperator variability; this value is 21.80% and 3.21% for operator 2 and 3, respectively. The interoperator variability is 19.08%.

Table 2
Intra- and Interoperator Variabilities for 12 Scans

	Slice 10				Slice 11				Slice 12			
	Intraoperator				Intraoperator				Intraoperator			
	Exp_A	Exp_B	Exp_C	Interoperator	Exp_A	Exp_B	Exp_C	Interoperator	Exp_A	Exp_B	Exp_C	Interoperator
Rat 1	43.96%	42.80%	20.45%	37.98%	9.10%	17.07%	13.44%	13.98%	12.15%	20.00%	11.20%	16.51%
Rat 2	8.38%	14.81%	22.77%	19.92%	9.92%	15.30%	12.19%	12.67%	18.07%	18.07%	16.39%	15.18%
Rat 3	22.44%	12.03%	17.18%	19.67%	6.12%	11.65%	2.79%	9.38%	10.21%	9.01%	19.25%	12.58%
Rat 4	6.50%	11.63%	4.18%	12.98%	3.49%	11.96%	8.59%	11.13%	15.19%	10.18%	6.13%	15.21%

The mean coefficient of intraoperator variation of is 13.74%; the mean coefficient of interoperator variation 16.43%.

Each expert (Exp) A, B, and C segmented the stroke area three times on different days. Intra- and inter-coefficient of variations are computed.

missed by the segmentation results (Fig 8). Figure 7 shows the segmentation results from 12 rat MR imaging scans. Table 3 includes the accuracy measures for all 12 scans. The mean TPVF of our method is 0.8877 (95% CI 0.7254 to 1.0500); the mean FPVF is 0.3370 (95% CI −0.0893 to 0.7633); the mean FNVF is 0.1122 (95% CI −0.0502 to 0.2747).

Assessment of Efficiency

Efficiency is important when there are a larger number of scans in clinical settings. The average operating time for each expert delineating stroke regions per volume (eight image slices) was 20 ± 5 minutes. In contrast, the automated algorithm took about 2 ± 0.5 minutes in a MATLAB computing environment.

DISCUSSION

We propose a fully automated method for detection and segmentation of acute/subacute ischemic stroke, based on the inherent bilateral symmetry of the brain. This technique has been demonstrated and validated on MR images of rodent cerebral ischemic stroke and compared with post-mortem histologic sections. Preliminary use of this method has also been tested in the setting of human acute stroke (24).

We make use of statistical analysis on paired windows across hemispheres that leverage the fact that the brain is grossly symmetrical. In cases where the difference between the two square-windowed populations is statistically significant, a pathologic condition is sug-
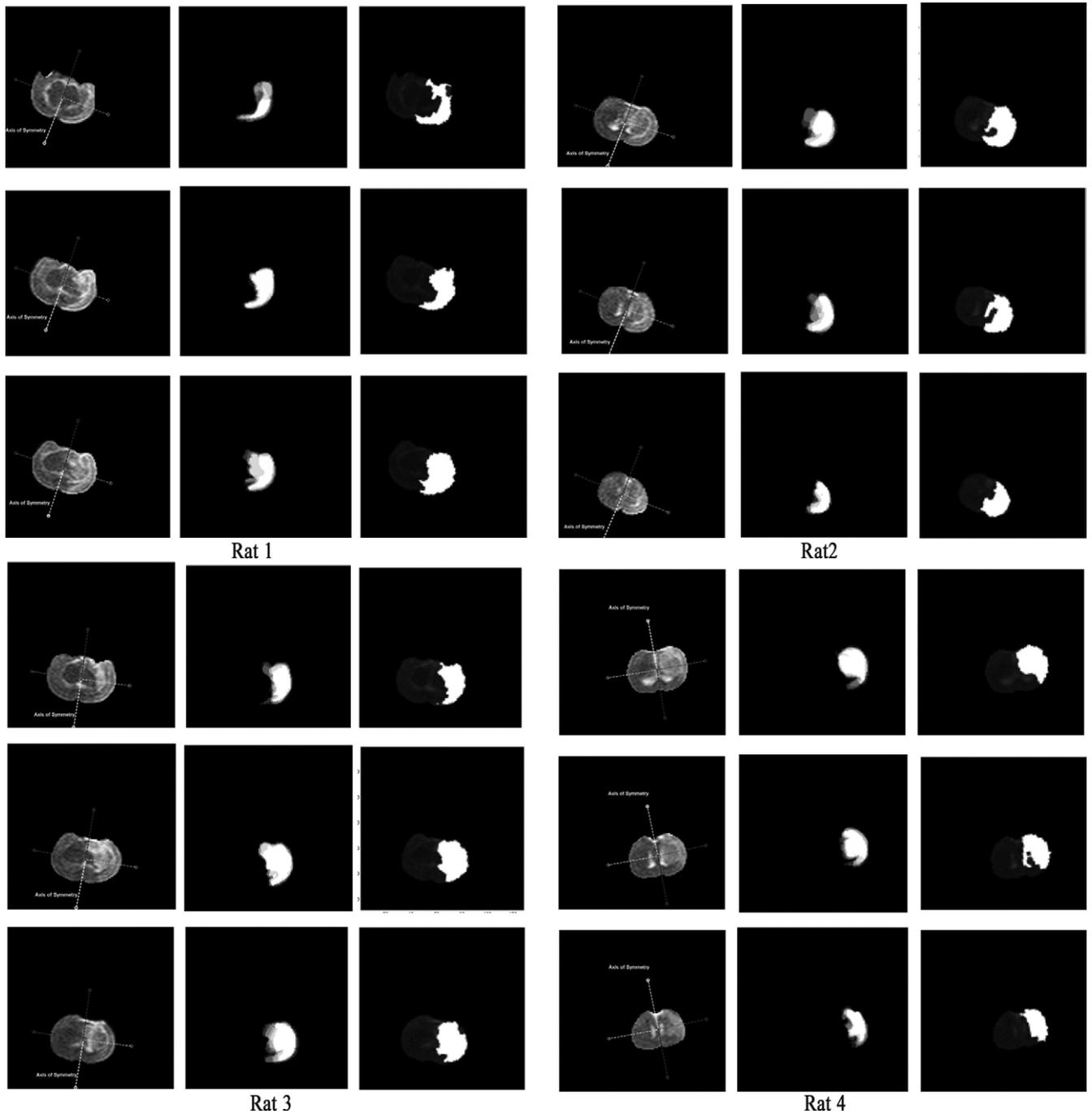
Figure 7. Validation of ischemic stroke segmentation in the rat cerebral ischemia cases, acquired with magnetic resonance imaging. In each group of nine images representing one rat study, the left-most column is the original brain with identified symmetry axes; the second column is the surrogate ground truth of the stroke region, and the third column contains the final segmentation results using our algorithm.

gested. From this observation we derive a fully automated segmentation method of gross brain pathologies.

Because the detection of the symmetry axis is based on the correct inclusion of a structure of interest (in our case the brain), the delineation and separation from other redundant structures is critical to the performance. In the Methods section, we describe how non-brain tissue can be excluded by applying a small δ, the background cutoff
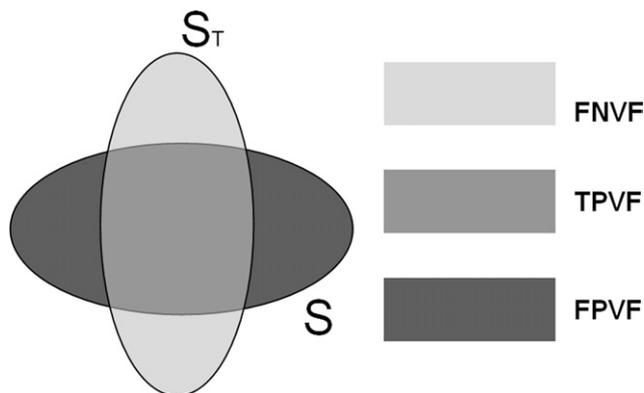
Figure 8. A geometric illustration of the three accuracy factors for manual delineation of a stroke region. S_T and S are sets of pixels representing segmentations from the ground truth and our algorithm. Accuracy is measured by three metrics: truth-positive volume fraction (TPVF), false-positive volume fraction (FPVF), and false-negative volume fraction (FNVF).

value that separates background intensity from brain tissue intensity. We note that this method should be approached with caution. We set δ a less conservative value—a value higher than 5 SDs from the mean background intensity. By doing so, the background can be discarded completely, and, in addition, some inner structures of the brain may also be removed because of their intensity overlap with that of the background. However, as our method focuses on discovering the symmetry axis of the global shape of an object, the performance remains unaffected, although some interior pixels in the brain region are omitted from the computation. Internal content asymmetries commonly lead to the pitfalls in a registration-based, mid-line detection method. The advantage of employing shape symmetry as a criterion to compute the symmetry axis is manifested by its performance consistency, regardless of the presence of content asymmetries. Although we use a simple method to extract background, there has always been an option of using commercial tools to separate the brain from the other structures in MR images.

Nevertheless, small errors in primary detection of the symmetry axis might impair the accuracy of the secondary operation (ie, the asymmetry quantification between hemispheres). To increase the systematic tolerance to the minor errors introduced by symmetry axis detection, we consider adopting the following compensation algorithms when conducting pairwise statistic comparisons: 1) we form two square windows symmetrically about the symmetry axis (as described in the Methods section); and 2) instead of one-to-one comparisons, we perform one-to-

many comparisons between the population from one window to that of the corresponding window and its *vicinity window;* then, record only the smallest P value. This adjustment has the potential to correct the error when the estimated symmetry axis has κ number of pixels off the true axis. The searching space for the minimal P value should be extended to *the vicinity* of the opposing window of a radius κ. This enhancement may help to handle more complex data input. For example, if the brain image has been somehow skewed and symmetry axis no longer appears as a straight line, the allowance of a small shift may provide our algorithm with a better tolerance to the bias in symmetry axis identification.

Two types of difference maps, namely the SDM and the ADM, are used to store two classes of asymmetry information. The former records the statistically significant difference by employing a very small α (the level of significance) to ensure the validity of the seeds, such that it strictly excludes the nonstroke region. The latter represents a gross picture of the left–right difference between hemispheres. Therefore, it contains both stroke asymmetries as well as many artifacts. Thus, the SDM is an undersegmentation of a stroke region, whereas the ADM is an oversegmentation. By assuming that the true stroke region is geographically eight-way connected and that all artifacts are not representing the actual stroke, the region growing technique should be able to capture the essential stroke region by expanding the core stroke from SDM. All the artifacts are no longer of concern because they are removed as disconnected components. The strength of this technique exists in full automation of generating seeds from an asymmetry computation. A simple region growing technique to grow the seeds is used, although other possible solutions, such as deformable model and fuzzy connectedness, might produce similar or even better delineation results. The proposed region growing technique, however, has been sufficient to generate qualitatively and quantitatively satisfactory results in the current rat stroke models. When the asymmetric artifacts are adjacent to the boundary of the lesions, additional errors might occur. Although this does not pose a significant issue in the current rat stroke MRI images, in other medical applications, it is conceivable that this could degrade optimal performance. One solution could be the fusion of the ADM and the original brain image, which will be treated as a cross-referenced seed mask. This will help avoiding any connected artifacts that could exhibit similar signal intensities as that of a lesion and also to ignoring

Table 3
Accuracy Measurement of the Automated Segmentation Method

	Slice 10			Slice 11			Slice 12		
	TPVF	FPVF	FNVF	TPVF	FPVF	FNVF	TPVF	FPVF	FNVF
Rat 1 (S2)	0.822	0.7787	0.1779	0.962	0.2697	0.0382	0.993	0.3563	0.0067
Rat 2 (S2)	0.948	0.7526	0.0515	0.803	0.1375	0.1973	0.722	0.2997	0.2776
Rat 3 (S2)	0.880	0.3622	0.1199	0.847	0.1549	0.1530	0.974	0.3689	0.0256
Rat 4 (S2)	0.915	0.1451	0.0848	0.837	0.1757	0.1634	0.949	0.2431	0.0510

FPVF: false-positive volume fraction; TPVF: true-positive volume fraction;
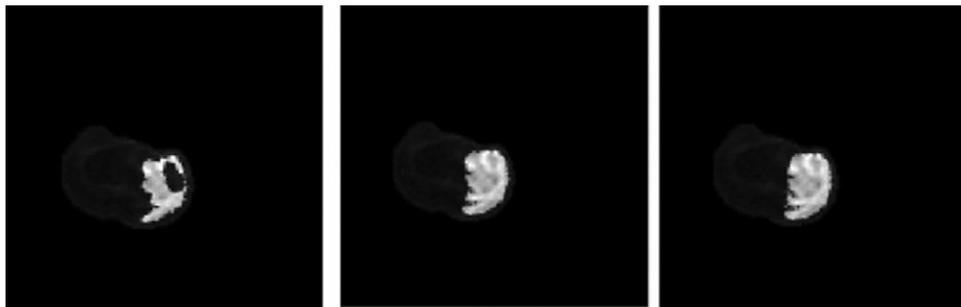
Figure 9. The statistical difference map (SDM) computed with different window sizes. From left to right, the window sizes are 5, 7, and 9 pixels, respectively. The α value (ie, level of significance) is fixed as 5.0770e-09.

any asymmetric artifacts that may be adjacent to asymmetric pathologies.

As far as parameters are concerned, two independent variables need to be justified.

1. *The window size for conducting statistic tests*: As we set the squared window unit for nonparametric tests, we select a fixed size of the window. With the window's increased size, each statistical sample unit contains more elements, and the sensitivity in terms of its inability of spotting small asymmetries is decreased. Howerver, with the increased sample size, the test becomes more powerful. Therefore, for larger window size, its type II error (if we accept the null when it is false) actually decreases. For the ischemic brain stroke application, we selected a 7×7 window as a tradeoff between sufficient sample size (49 for each window), and maintaining a reasonable statistical power in the nonparametric test (Fig 9).
2. *The α value, the level of significance, for rejecting or accepting the null hypothesis*: We start with an arbitrary α value obtained from an empiric study upon existing rat MR imaging data. We select an

empiric small α value because it has been observed that it can provide expected results. We have noticed that as long as the α falls into a certain range, its specific value is less relevant, because a secondary threshold is selected for further trimming of the SDM. The rule of thumb is that the α value should be small enough for the exclusion of most artifacts resulting from the normal asymmetries or geometric misalignment. A small α value tends to undersegment the region of interest, but undersegmentation is better than oversegmentation, because the former can be further expanded via a region growing technique, whereas the removal of an oversegmented region is far more difficult.

The validity of the current segmentation algorithm, in stroke detection of rat ischemia, and its potential in other clinical image applications, are demonstrated. A fully automated symmetry-based paradigm to assist in the detection of brain pathology is proposed. One might question how this method would perform if a brain lesion were to cross the mid-line or a pair of brain lesions was largely bilaterally symmetrical. The ability of our algorithm to handle these issues is illustrated in a diagram (Fig 10),

Original image   Statistical Difference Map
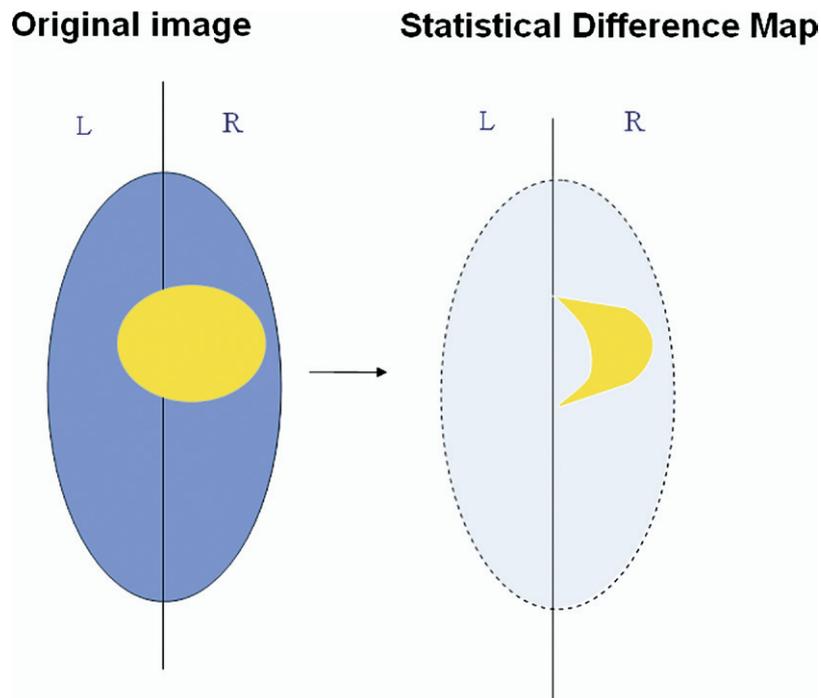
Figure 10. An illustration of dealing with a brain lesion crossing the symmetry axis (left image). We can discover the dissimilarities and characterize them as seeds (shown as the *wedge* on the right image) via a pairwise statistical test; thus, the symmetric portion of the lesion has mostly been canceled out.

where a big lesion is seen to cross the midline. If this lesion is largely homogeneous, the dissimilarities can be discovered via a pairwise statistical test; the symmetric portion of the lesion is mostly canceled out. This process yields the statistical difference map (or seeds map) characterized by the statistically asymmetric fraction of the entire lesion. As long as this mid-line lesion or bilateral lesions are not perfectly symmetric (perfectly symmetric lesions being generally uncommon—eg, rare metabolic disorders), there will always be some initial placement of seeds marked as a asymmetric fraction of the lesions. After seeds are correctly drawn, the region growing technique will enclose other connected components until the entire lesion is labeled.

Although the evaluation study on rat ischemic stroke models has demonstrated a high level of accuracy, a question remains on how sensitive this methodology can be in identifying smaller lesions. We have identified four major types of asymmetries in brain images: 1) normal asymmetry in signal intensity, 2) abnormal asymmetry in signal intensity (eg, the presence of tumor), 3) noise from geometric misalignment, and 4) noise from inhomogeneity of the signals (eg, bias fields). Type 1 asymmetry is generally statistically less significant than type 2 asymme-

try. Types 3 and 4, however, may maliciously affect the performance of the symmetry-based approach, because the statistical test may find those differences even more significant than the pathologic differences. For type 4, we are examining the alternatives to remove the noise as a preprocessing step. For types 1 and 3 asymmetries, hemisphere-wise cross-egistration may be the solution. Because we want to address both intensity variances and geometric misalignments between two hemispheres, we can choose an intensity-based approach to avoid various pitfalls related to feature selection. We have modeled the transformation with a local affine model and a global smoothness constraint, based on a known algorithm (25). This allows us to capture nonlinear distortions in both geometry and intensity. This entire procedure is built on a differential framework, and the standard mean square error metric on the intensity values is employed (26).

Although our three operators were all trained medical technicians and they delineated the stroke region with the help of histologic images, a big variation in their segmentation results was reflected by a large-valued coefficient parameter—the intra- and interoperator CV, as discussed in the early work (12). This is partly because the stroke regions in the MR image rat model fail to assume clear

(a)   (b)   (c)   (d)
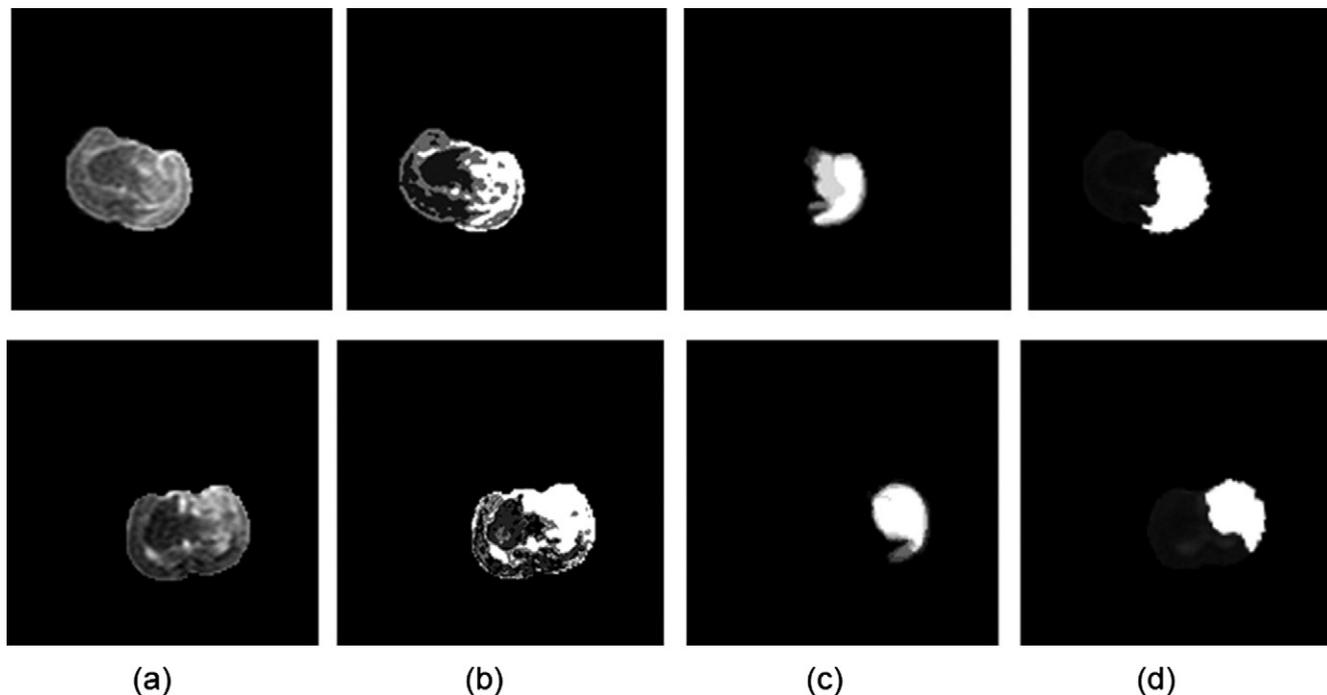
Figure 11. Comparison of segmentation results of stroke magnetic resonance imaging data from rats **(a)** using the level set method **(b)**. Ground truth and segmented stroke using symmetry-based method are depicted in **(c)** and **(d)**, respectively. Level set segmentation, although it automatically classifies the brain tissue into four major classes, misclassifies some normal tissues (on the healthy side of the brain) signally overlapping with that of stroke (illustrated in *white* signals in **b**).

boundaries and the outline fuzziness makes it difficult for the operators to precisely delineate the stroke region. This leads to questionable fidelity in generating surrogate ground truth. The accuracy measurement therefore is affected because the computation of accuracy measures depends on quality of delineations from which surrogate ground truth is derived. Another reason contributing to the relatively low-accuracy results is that the rat brain is very small and a minor delineating error may result in a relatively large false-positive or false-negative outcome in the accuracy study. These factors explain why the TPVF is not close to 1, nor the FPVF and the FNVP close to zero, as shown in Table 3.

Another limitation comes from the large slice thickness in the volumetric MR data, which cannot be treated as a volume. In our method, we processed each individual slice in the MR data and we could not make use of volumetric information that would definitely improve the final result. Thus, the ischemic stroke regions were studied independently, slice by slice, under the assumptions that all the slices were approximately well-aligned in the coordinate system. By not being able to take the 3D information into account, asymmetry computation became highly subject to global misalignment errors. In other studies, we

have been computing the 3D symmetry plane of the brain (27) and discovering the volumetric asymmetric patterns, using the same framework discussed in this work.

Despite potential issues, as previously discussed, our method exhibits superior performance compared to the state-of-the-art methodologies in brain pathology segmentation. Conventional region-based segmentation methods are statistical in nature. They typically require supervised learning and a priori information from manual labeling or from an atlas. On the high end of sophisticated region-based segmentation, a framework called fuzzy connectedness has shown considerable promise in dealing with noisy images with intrinsic artifacts such as blurring (partial volume effects), noise, and background variation (28). This yields more precise segmentation results; however, the simply fuzzy connectedness algorithm requires the operator to select a seed to initialize the algorithm. Compared to the CV method, the symmetry-based method enjoys an advantage that it does not require the manual seeding. That said, in many clinical images with nontrivial signal inhomogeneity and noise, it would be interesting to combine symmetry-based methods with CV, because the former automatically identifies and extracts the region of interest by contrasting one half from the

other, providing a mechanism for seed initialization, whereas the latter offers a sophisticated region growing technique. This hybrid method could be a win-win combination that is likely to perform more robustly without the need of minimal operator intervention.

Other than region-based methods, boundary-based methods, such as level set (ie, geometric deformable model) have many advantages. In an earlier work (29), a multiphase 3D level set algorithm performed a minimal partitioning of data into piecewise constant objects. In this method, random seed initialization was used to minimize the sensitivity of the method to initial conditions while avoiding the need for a priori information. The level set implementation framework for surface propagation offers the advantages of easy initialization, computational efficiency, and full automation in segmenting normal 3D brain MR imaging. The proposed energy function is defined in Equation 7 as the following:

$$\frac{\partial \phi}{\partial t} = \delta_t(\phi) \left[\mu div \left(\frac{\nabla \phi}{|\nabla \phi|} \right) - \nu + \lambda_1 |u_0 - c_1|^2 \right.$$
$$\left. - \lambda_2 |u_0 - c_2|^2 \right]. \quad (7)$$

where $c1$ is object value, $c2$ is the background value, and $\mu, \nu, \lambda1, \lambda2$ are fixed parameters.

Because the exterior growing force for segmenting a volumetric data ($u0$) is still largely dominated by the intensity homogeneity, this may lead to misclassification between tissues that assume an intensity overlap. This is observed between stroke and normal tissue in the rat ischemia MR image dataset. We provide the segmentation results using level set program multiphase 3D level set (Fig 11b). Compared to the ground truth (Fig 11c) and symmetry-based segmentation method (Fig 11d), the stroke region (illustrated in white signals in Fig 11b) "permeated" into another hemisphere where the signals are considerably similar with that of stroke.

CONCLUSION

We present a fully automated methodology, a pipeline of operations, to detect, segment, and quantify ischemic acute/subacute stroke regions in rodent brain imagery, using brain hemispheric asymmetry as the principal feature to distinguish abnormal tissue from normal tissue. This approach consists of identifying the axis of symme-

try, measuring and localizing asymmetries between hemispheres, and statistical modeling and classifying of the difference map. The preliminary results have shown that this approach has the potential to achieve high accuracy and full automation in segmenting gross pathologies in bilaterally symmetric brain tissue. Automated quantification of the presence and degree of asymmetries in brain MR images could assist future clinical assessments using computer-aided diagnostic software. Although we focus on illustrating the capability of our method mainly with ischemic stroke cases in a rat model, this fully automated approach might be generalized to asymmetry quantification of other brain pathologies, and possibly to other applications, such as face recognition, where the anatomic structures are recognized as grossly symmetric under normal conditions.

REFERENCES

1. American Heart Association. Heart disease and stroke statistics, 2006. Available at: http://www.americanheart.org/presenter.jhtml?identi-fier=1928. Accessed December 20, 2006.
2. Pham D, Xu C, Prince J. Current methods in medical image segmentation. Ann Rev Biomed Engineering 2000; 2:315–337.
3. Kaus MR, Warfield SK, Nabavi A, et al. Automated segmentation of MR images of brain tumors. Radiology 2001; 218:586–591.
4. McInerney T, Terzopoulos D. Deformable models in medical image analysis: a survey. Med Image Anal 1996; 1:91–108.
5. Udupa J, Leblanc V, Schmidt H, et al. Methodology for evaluating image-segmentation algorithms. SPIE 2002: 266–277.
6. Clarke LP, Velthuizen RP, Phuphanich S, et al. MRI: stability of three supervised segmentation techniques. Magn Reson Imaging 1993; 11: 95–106.
7. Clark MC, Hall LO, Goldgof DB, et al. Automatic tumor segmentation using knowledge-based techniques. IEEE Trans Med Imaging 1998; 17:187–201.
8. Thirion JP, Prima S, Subsol G, et al. Statistical analysis of normal and abnormal dissymmetry in volumetric medical images. Med Image Anal 2000; 4:111–121.
9. Volkau I, Prakash B, Ananthasubramaniam A, et al. Quantitative analysis of brain asymmetry by using the divergence measure: normal-pathological brain discrimination. Acad Radiol 2006; 13:752–758.
10. Bederson JB, Pitts LH, Germano SM, et al. Evaluation of 2,3,5-triphe-nyltetrazolium chloride as a stain for detection and quantification of experimental cerebral infarction in rats. Stroke 1986; 17:1304–1308.
11. Harvard apparatus. Available at: http://www.harvardapparatus.com/. Accessed June 10, 2004.
12. Imielinska C, Rosiene J, Jin Y. Ground truth for evaluation of ischemic stroke hybrid segmentation in a rat model of temporary middle cerebral artery. Comp Assist Radiol Surg 2005; 1281:74–79.
13. Bigun J. Recognition of local symmetries in gray value images by harmonic functions. ICPR. 1988; 1:345–347.
14. Gofman Y, Kiryati N. Detecting symmetry in grey level images: the global optimization approach. Proceedings of the 13th International Conference on Pattern Recognition 1996: A94.2.

15. Reisfeld D, Wolfson H, Yeshurun Y. Context free attentional operators: the generalized symmetry transform. IJCV 1995; 14:119–130.

16. Liu X, Imielinska C, Rosiene J. A novel quantification method for determining previously undetected MR perfusion changes in patients with cognitive deficits following carotid endarterectomy. SPIE 2005; 5747: 796–805.

17. B. Klaus PH. Robot vision. Cambridge, MA: MIT Press; 1986.

18. Imielinska C, Liu X, Sughrue M, et al. Objective quantification of perfusion-weighted computer tomography in the setting of acute aneurysmal subarachnoid hemorrhage. Comp Assist Radiol Surg 2004; 1268:34–43.

19. Imielinska C, Liu X, Rosiene J. Towards objective quantification of perfusion- weighted computed tomography in the setting of subarachnoid hemorrhage: quantification of symmetry and automated delineation of vascular territories. Acad Radiol 2005; 12:874–887.

20. Lehmann EL. Nonparametric statistical methods based on ranks. New York: McGraw-Hill; 1975.

21. Rafael C, Gonzalez REW. Digital image processing. Ed 2. New York: Prentice Hall; 2002.

22. Imielinska C, Jin Y, Liu X, et al. Evaluation of ischemic stroke hybrid segmentation in a rat model of temporary middle cerebral artery occlusion using ground truth from histologic and MR data. SPIE 2005.

23. Udupa JK, Leblanc VR, Zhuge Y, et al. A framework for evaluating image segmentation algorithms. Comp Med Imaging Graph 2006; 30: 75–87.

24. Tulipano PK, Millar W, Imielinska C, et al. Quantification of diffusion weighted images (dwi and apparent diffusion coefficient maps (ADC) in detection of acute stroke. SPIE 2006.

25. Periaswamy S, Weaver JB, Healy DM Jr., et al. Differential affine motion estimation for medical image registration. SPIE 2000; 1066–1075.

26. Liu X, Ogden RT, Imielinska C, et al. Statistical bilateral asymmetry measurement in brain images. IEEE 2006 International Conference of the Engineering in Medicine and Biology Society. New York; 2006. p. 1441–1145.

27. Liu X, Imielinska C, Laine A, et al. Symmetry identification using partial surface matching and tilt correction in 3D brain images. IEEE 2006 International Conference of the Engineering in Medicine and Biology Society. New York; 2006. p. 1056–1060.

28. Udupa JK, Samarasekera S. Fuzzy connectedness and object definition. SPIE 1995; 2–11.

29. Angelini E, Song T, Mensh B, et al. Brain MRI segmentation with multiphase minimal partitioning: a comparative study. Intl J Biomed Imaging 2007; 2007:10526.